JOURNAL OF MATERIALS SCIENCE 10 (1975) 846–856

Slow crack growth in graphite

P. H. HODKINSON, J. S. NADEAU
Department of Metallurgy, University of British Columbia, Vancouver, Canada

Slow crack growth tests on isotropic graphite and pyrolytic graphite at room temperature have revealed a stress intensity-crack velocity behaviour similar to the third stage of crack growth in soda-lime glass. Thus, it appears that graphite undergoes failure at room temperature only at large fractions of the critical stress intensity. Considerable difference in fracture behaviour of graphites having different microstructures was observed. Slow crack growth occurred more readily at 500° C than at room temperature, suggesting an environmental effect.

1. Introduction

Graphites are being used increasingly for load-bearing applications in high temperature environments so that long-term performance of these materials under such conditions is important. In some ceramics, delayed failure can occur by the slow growth of subcritical cracks, a process which is normally sensitive to environment.

Time-dependent failure of graphite was first reported by Diefendorf [1], who measured a consistent 10% decrease in the room temperature strength of a commercial petroleum coke graphite on applying strain-rates less than 10^{-3} sec^{-1}. Also, half the strength increase caused by raising the temperature to 1000° C was retained at room temperature if the specimen was kept in a high vacuum. Admission of air reduced the strength to the original value.

Wilkins [2] plotted static fatigue data for an extruded graphite as homologous stress versus time-to-rupture. He concluded that at room temperature, delayed failure of extruded graphite occurs only at a value of the applied stress which is a large fraction of the instantaneous strength.

Simpson [3] performed slow crack growth tests on isotropic graphite using the double torsion technique to obtain stress-intensity-crack velocity diagrams both in air and toluene at room temperature. The toluene apparently increased the resistance of the isotropic graphite to slow crack growth. In both cases only a single stage K_I-V curve was observed.

In the present study the microstructural features controlling slow crack growth in graphite were investigated. The fracture mechanics approach was followed in which delayed failure is described by the crack velocity-stress intensity factor diagram [4]. The double torsion technique was used to generate V-K_I plots for several graphites at room temperature and for one graphite at 500° C.

2. Experimental procedure

2.1. Materials selection

Two grades of porous graphite*, (31% and 18% pores) having a maximum particle size of about 25 μm were used. Wagner *et al.* [5] have confirmed that the same starting materials are used for all POCO graphites and that for this series of graphites the primary variable is the density. In contrast to POCO, pyrolytic graphite† was chosen as an example of a dense, well-ordered anisotropic graphite.

2.2. Structural characterization

Several techniques were used to investigate the pore structure of the graphites. Bulk density measurements were made by immersion in water and after coating samples with paraffin wax. The density was also measured with a helium-air pycnometer. The volume distribution of macropores in the isotropic graphites were determined by mercury porosimetry using small rectangular blocks containing ~ 0.2 cm^3 open pores.

All materials were examined with a light microscope to observe differences in microstructure. Specimens were vacuum impregnated with epoxy resin and then mounted, metallo-

*Poco Graphite, Decatur, Texas, grades AXZ (~ 31% porous) and AXF-5Q (~ 18% porous).
†Electronic Space Products Inc, Los Angeles, California.

graphically ground and polished using silicon carbide powder; the final polish was accomplished with a slurry of 0.05 μm alumina in a 10% aqueous solution of hydrogen peroxide [6].

2.3. Young's modulus

A standard mechanical resonance technique [7] was used to measure the Young's modulus of rods of isotropic graphite vibrated in the flexural free-free mode. Four samples of each grade were prepared, 200 mm × 9 mm × 6 mm and the Young's modulus, E, was calculated from the first mode resonance frequency. Values of E were corrected for the effects of shear displacement and rotatory inertia as outlined by Pickett [8].

2.4. Slow crack growth tests

A simple and reliable method for slow crack growth studies is the double torsion technique [9, 10]. The important feature of this test is that the stress intensity, K_I is independent of crack length so that the crack does not propagate unstably under constant load.

Specimens consisted of simple rectangular plates, 76 mm × 25 mm × 3 mm, with a 1.5 mm deep guide groove and slotted at one end to a depth of 10 mm. An enlarged view of a typical specimen is shown in Fig. 1. The loading fixture has been described elsewhere [11].

Stress intensity-crack velocity data were obtained by the load relaxation method. A sharp crack was initiated at the end of the slotted notch with a razor blade. The specimen was loaded in a testing machine* to accelerate the crack, the cross-head was stopped and the load relaxation recorded on the chart recorder.

The stress intensity factor at a particular load, P, was calculated from the equation:

$$K_I = PW_m \left(\frac{3(1+\nu)}{Wt^3 t_n}\right)^{1/2} \quad (1)$$

where W_m = momentum, W = specimen width, t = specimen thickness, t_n = web thickness, ν = Poisson's ratio.

The crack velocity at the particular load, P, was computed from the rate of load relaxation (at constant displacement) and the final crack length using the equation:

$$V = -\phi \frac{P_f}{P^2}\left(a_f + \frac{D}{B}\right)\left[\frac{dP}{dt}\right]_y \quad (2)$$

*Instron Corp., Canton, Ma.

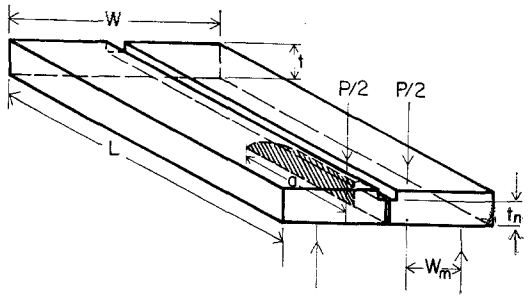

Figure 1 A double torsion specimen.

where ϕ = geometrical factor, P_f = final load at the end of load relaxation, a_f = final crack length, $B = dC/da \approx [6W_m^2(1+\nu)]/Wt^3E)$ = slope of the compliance calibration, D = intercept of the compliance plot for zero crack length and y is the specimen deflection.

A compliance calibration was performed to obtain experimental values of the slope B and the intercept D. Notched specimens of each material were used, the notch being successively lengthened after each compliance measurement.

In general, the following procedure was carried out for the load relaxation tests:

(1) Each specimen was loaded incrementally at a cross-head speed of 8.5×10^{-8} m sec^{-1} (0.0002 in. min^{-1}) until a rapid load drop and relaxation curve was obtained. This indicated the formation of a sharp crack.

(2) The load was increased at a cross-head speed of 8.5×10^{-7} m sec^{-1} (0.002 in. min^{-1}) to accelerate the crack and a second load relaxation curve was produced.

(3) When the load had decreased to a sufficiently low value the specimen was removed from the fixture and the final crack length measured (see later).

(4) The sample was reloaded to reproduce the load relaxation curve and then fast loaded at a crosshead speed of 2×10^{-4} m sec^{-1} (0.5 in. min^{-1}) to failure, for the determination of the critical stress intensity factor, K_{IC}.

Room temperature tests in air were performed on all three graphites, the basal planes of the pyrolytic graphite were oriented parallel to the largest flat surfaces of the specimen. Also, 50 mm long specimens of isotropic graphite were tested at 500°C in a nichrome wound resistance furnace; specimens were allowed approximately 1½ h to equilibrate prior to testing. Temperatures were controlled to ± ½°C.

2.4.1. Observation of the crack length and profile

A dead weight loading apparatus set up with a travelling microscope was used to measure crack lengths in graphite. Specimens were torsionally stressed to some load below the final P_f value after load relaxation, and the crack opening was observed visually. Secondary cracking was evident close to the crack tip. Cracks could only be observed on one side of the specimen, the side that opened on loading. Therefore, the crack profile could not be ascertained by this technique. Because of this the crack front was assumed to be planar, taking the geometrical factor, ϕ, in Equation 2 as unity.

2.4.2. Machine relaxation

Machine relaxations were minimized by using a stiff load cell, by installing an "integral defeat" switch on the testing machine and by adding weights to the crosshead to prevent it from "floating up" when it was suddenly switched from "downward travel" to "stop". Most of the remaining background was removed by loading specimens to a load below the final value of P, P_f, and leaving the apparatus for 10 min.The rest of the background was taken into account in the calculation by obtaining a load relaxation curve at a load just below P_f. Exactly the same fast load procedure was followed for the background as for the true load relaxation curve which was obtained afterwards. The resultant background curve was then subtracted from the true load relaxation curve for a moving crack. Thus the lower limit of the velocity measurement was determined by the slope of the background relaxation. The uncertainty in the velocity for the lowest points plotted is about a factor of two.

2.4.3. Fractography

Fracture surfaces were examined by scanning electron microscopy.

3. Results and calculations

3.1. Structural characteristics

The results in Table I show that the bulk densities of the isotropic graphites were very reproducible. POCO AXZ is almost twice as porous as grade AXF-5Q (31.0% compared with 17.6%, respectively); however, this appears to be due mainly to differences in open porosity since the closed porosities are similar (2 to 3%). According to Wagner *et al.* [5] the open or interparticle pores result from incomplete filling of the interparticle packing voids and from shrinkage and gas evolution during binder pyrolysis. The filler-particle or closed pores exist mainly as basal plane delaminations resulting from local stresses introduced by the anisotropic expansion and contraction of particles during heat-treatment.

The mercury porosimetry results are listed in Table II. For the pore diameter calculated, a wetting angle of 130° for mercury on graphite and surface tension of mercury of 485 × 10^{-3} N m^{-1} were used. The difference in total open pore volume between samples "A" and "B" of grades AXZ and AXF-5Q are real and represent a variation of $\sim 7\frac{1}{2}\%$ and $\sim 3\%$, respectively. Both differences appeared to arise from changes in the volume of mercury intruded at pore sizes $\leqslant 0.7$ μm, and must be due to variations

TABLE I Densities and porosities of graphite at room temperature (based on theoretical density = 2.25 × 10^3 kg m^{-3})

	POCO AXZ	POCO AXF-5Q	Pyrolytic graphite
Bulk density (× 10^3 kg m^{-3})	1.552 ± 0.005 (4)*	1.854 ± 0.005 (4)	2.19 ± 0.02 (4)
Helium pycnometric density (× 10^3 kg m^{-3})	2.202 ± 0.008 (1)	2.180 ± 0.006 (1)	2.28 ± 0.03 (1)
Total porosity (%)	31.0	17.6	2.7
Closed porosity (%)	2.1	3.1	0
Open porosity (%)	28.9	14.5	2.7

* Number of measurements.

TABLE II Summary of results from mercury porosimetry

	POCO AXZ		POCO AXF-5Q	
	"A"*	"B"	"A"	"B"
Total open pore volume (× 10^{-3} m^3 kg^{-1})	0.195	0.21	0.0175	0.0695
Diameter of penetration (× 10^{-6} m)	0.8		0.95	

*"A" and "B" are two samples of the same nominal material.

TABLE III Elastic constants of graphite at room temperature

	POCO AXZ	POCO AXF-5Q	Pyrolytic graphite
Young's modulus (GN m^{-2})	7.1 ± 0.5 (4)*	13.4 ± 0.2 (4)	"a" direction 28-41‡
Poisson's ratio, ν	0.25†	0.15†	"a" direction −0.1‡
			"c" direction +0.9‡

*Number of measurements.
†Data sheet, Poco Graphite Inc, Decatur, Texas.
‡Data sheet, Electronic Space Products Inc, Los Angeles, California.

TABLE IV Summary of results from compliance calibrations

	POCO AXZ	POCO AXF-5Q	Pyrolytic graphite
Linear regression analysis equation: $c = \frac{y}{p} = Ba + D$*	$4.5 \times 10^{-5}a$ $+15.2 \times 10^{-7}$	$3.0 \times 10^{-5}a$ $+10.2 \times 10^{-7}$	$2.5 \times 10^{-5}a$ $+13.5 \times 10^{-7}$
Apparent E $E \approx \frac{6W_m^2(1+\nu)}{Wt^3B}$ (GN m^{-2})	13.4	18.7	"a" direction 20.8

*a is the crack length.

in the volume of closed pores relative to open pores as the total porosity for each grade has been established as uniform.

Optical microscopy showed the pores in isotropic graphite to be equiaxed and distributed more or less randomly throughout with no obvious preferred orientation. The pores varied in shape from almost circular to slits with a distribution of sizes up to a maximum of ~ 20 μm. In general, the observations corroborated the density and porosity results.

In comparison, pyrolytic graphite consists of groups of cones of graphite whose axes of symmetry are parallel, with the apex toward the substrate or nucleation site. The wrinkled nature of the basal planes is related to the roughness of the substrate and to the sootiness of the manufacturing process [12]. Examination in the optical microscope showed the cones to be several hundred microns across, with a finer scale cone-type structure occurring within each grain.

3.2. Young's modulus

The Young's modulus of the graphites at room temperature together with the manufacturer's values of Poisson's ratio are shown in Table III.

3.3. Slow crack growth tests

3.3.1. Compliance calibration

Fig. 2 indicates the constancy of the slopes of the compliance curves for crack lengths of at least half the specimen length. This confirms the general form of the analytical expression for the stress intensity factor used in these experiments. However, there is a discrepancy between the apparent Young's modulus calculated from the empirical equation (Table IV) and the dynamic Young's modulus. Since no explanation for this discrepancy is known the ratio D/B, necessary for materials with a high compliance, was not included in the crack velocity calculations.

3.3.2. Stress intensity factor-crack velocity diagrams

Typical load relaxation curves for the graphites are shown in Fig. 3. The total load drop during a relaxation was extremely small so that a highly sensitive load scale was required. A full scale load of 17.8 N (4 lb) was used in conjunction with a zero suppression, (scale expansion) capability.

The total distance of crack propagation in the relaxation of POCO AXZ B (Fig. 3b) was ~ 1.9 mm measured visually. The length of crack growth obtained by numerical integration of the relaxation curve was ~ 0.64 mm. Most of the crack growth occurs in the initial part of the relaxation where the resolution of the velocity is limited by the recorder pen speed, accounting in part for the larger value obtained visually. However, neither the correction factor, ϕ, nor

TABLE V Summary of results from K_I-V diagrams for graphites in air (linear regression analysis equation: $\log V = n \log K_I + \log A$).

Material and temperature	Equation	n	$\log A$	Origin of equation	K_{IC} (10^5 N $m^{-3/2}$)	$K_{IC}' = K_{IC}/(1-\rho)$ (10^5 N $m^{-3/2}$)
POCO AXZ R.T.	$\log V = 113 \log K_I - 662$ Overall crack growth process	113±32	−662±190	Mean equation for each specimen A, B, and D	7.3±0.5 (3)*	10.6
POCO AXF-5Q R.T.	$\log V = 218 \log K_I - 1343$	218±13	−1343±78	Regression analysis of all data prints	14.56±0.01 (3)	17.7
Pyrolytic graphite R.T.	$\log V = 216 \log K_I - 1384$	216±11	−1384±67	Mean equation for B and C	"a" direction 25.02±0.06 (2)	
POCO AXZ 500°C	$\log V = 63 \log K_I - 368$	63±16	−368±91	Mean equation for specimens A, B and C	6.4±0.4 (3)	9.3
POCO AXF-5Q 500°C	$\log V = 128 \log K_I - 789$	128±14	−789±88	Mean equation for specimens A, B, C and D	14.47 (1)	17.6

*Number of measurements

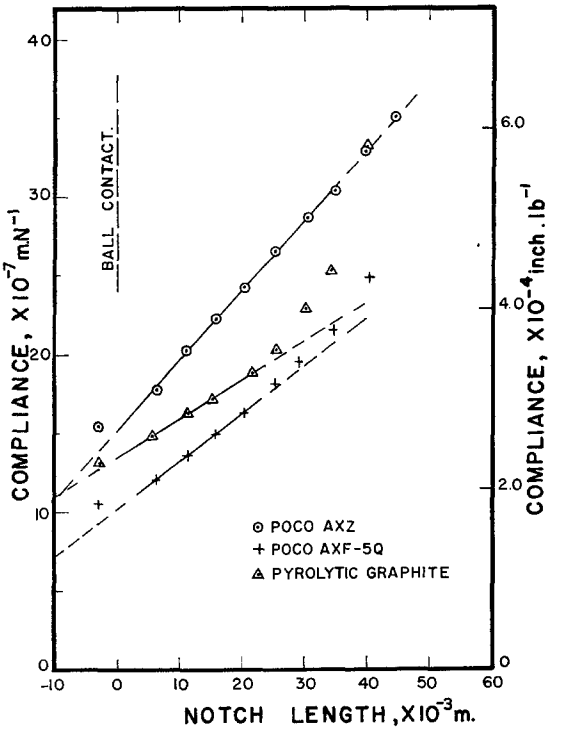

Figure 2 Compliance calibration for the three graphites.

the ratio, D/B, were included in the velocity calculation and both factors may have an effect.

The K_I-V diagrams calculated from the load relaxation curves are shown in Figs. 4 and 5 and the results summarized in Table V. Values of K_{IC} normalized for the effects of uniformly distributed porosity by dividing by $(1-\rho)$ where ρ is the fractional porosity, are also shown.

Although the K_I-V diagrams show considerable scatter, data points for POCO AXF-5Q at room temperature all lie within experimental error ($\sim 10.05 \times 10^5$ N $m^{-3/2}$).

For POCO AXZ at room temperature, a series of discontinuous K_I-V lines were obtained as the crack accelerated several times. These lines lie considerably to the left of the critical stress intensity.

At least two types of K_I-V curve were produced for pyrolytic graphite. A, A^1 and C, C^1 refer to separate load relaxations obtained on the same specimen. A slope of ~ 200 was generally obtained when the crack accelerated several times and the steeper slope of ~ 500 after only one acceleration, i.e. a single load relaxation. Unlike POCO AXZ, the load relaxation curves were extremely difficult to resolve.

Some difficulty was encountered in controlling the crack to move it accurately down the centre of the guiding groove. Control of the crack path was attained with POCO AXF-5Q with specimens grooved to half their original thickness. However, with POCO AXZ the crack tended to run along the side of the groove. The maximum experimental error due to the larger surface area exposed in this region is estimated to be -0.05×10^5 N $m^{-3/2}$. With pyrolytic graphite the

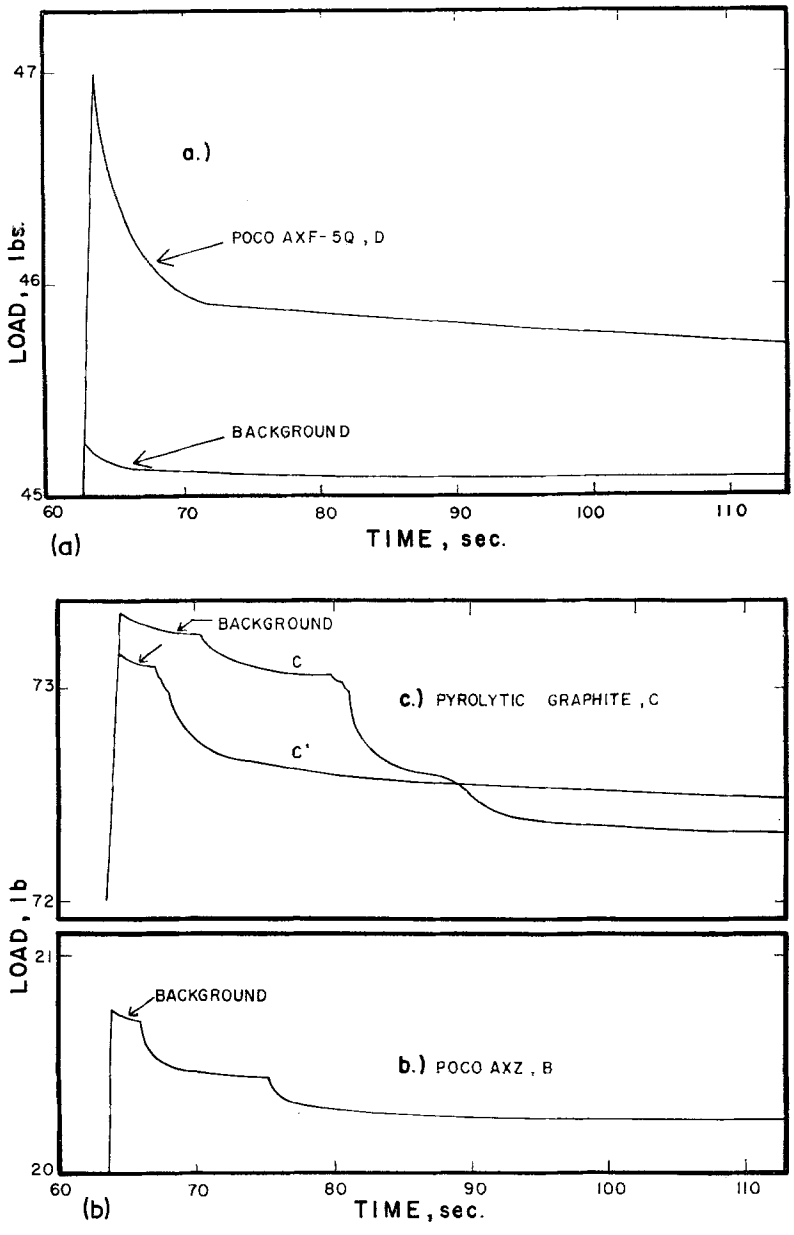

Figure 3 Typical load relaxation curves at room temperature: (a) POCO AXF-5Q, (b) POCO AXZ, (c) Pyrolytic graphite.

crack would initially move straight along the centre of the groove but on reloading a sample after a load relaxation measurement, the crack would twist and shear to one side of the specimen. The onset of this was generally marked by a long load relaxation on the chart recorder at a load below that corresponding to the first P_f value. Therefore, no values of K_{IC} were obtained for specimens A, B, or C. K_{IC} was determined using new specimens D and E, after load relaxing in the appropriate region and fast loading to failure. Study of the crack path afterwards revealed that the cracks were also crooked after fast loading.

The upper limit for the crack velocity was always determined by the cross-head speed

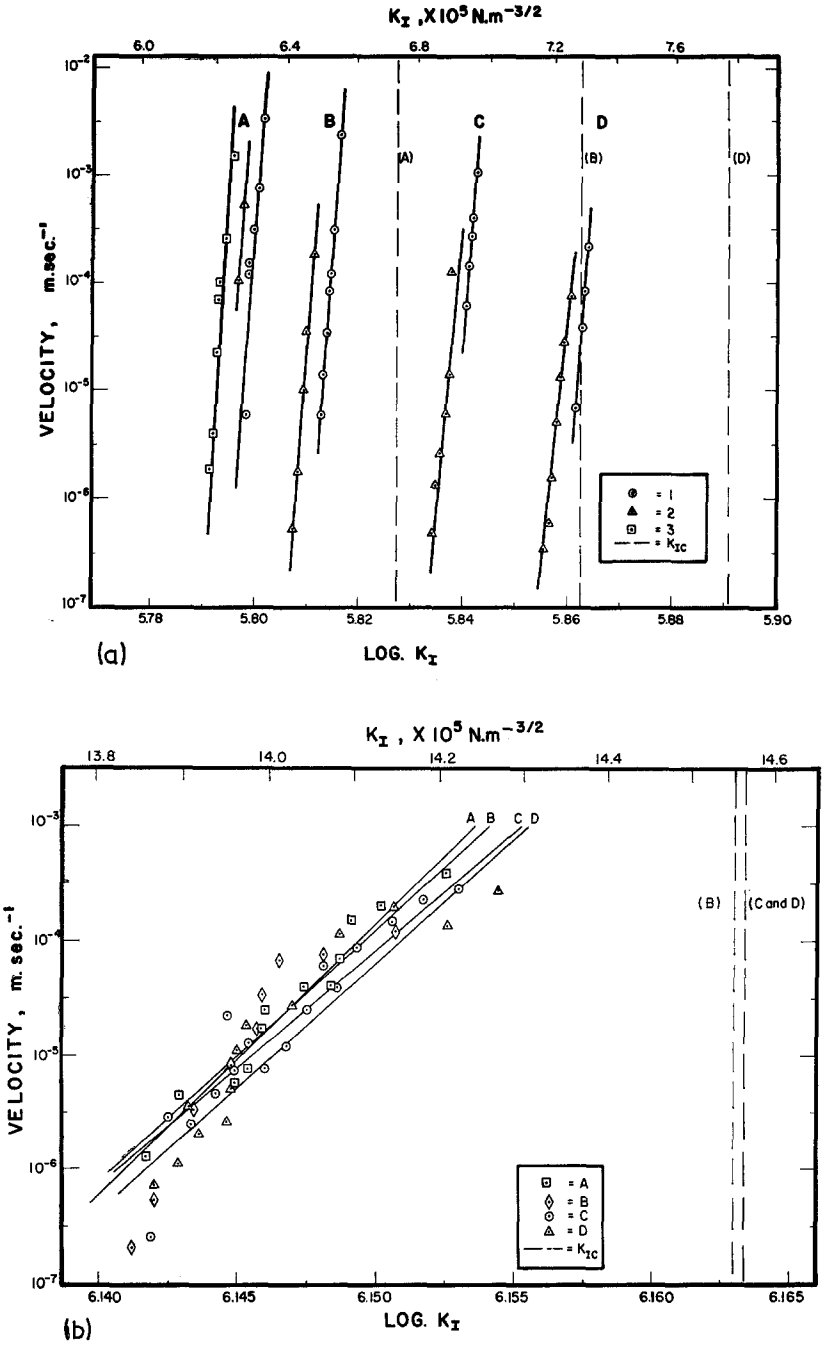

Figure 4

applied to the specimen prior to relaxation; the lowest velocity that could be measured was dictated by the background relaxation.

The crack velocity was recalculated to show the effect of the ratio D/B for the case of pyrolytic graphite, specimen C, and this is shown by the dotted dashed lines in Fig. 4c. The crack velocities are effectively increased by a factor of 5 resulting in a change in the intercept but no change in the slope of the K_I-V diagram. For the isotropic graphites the apparent correction factor was about 3.

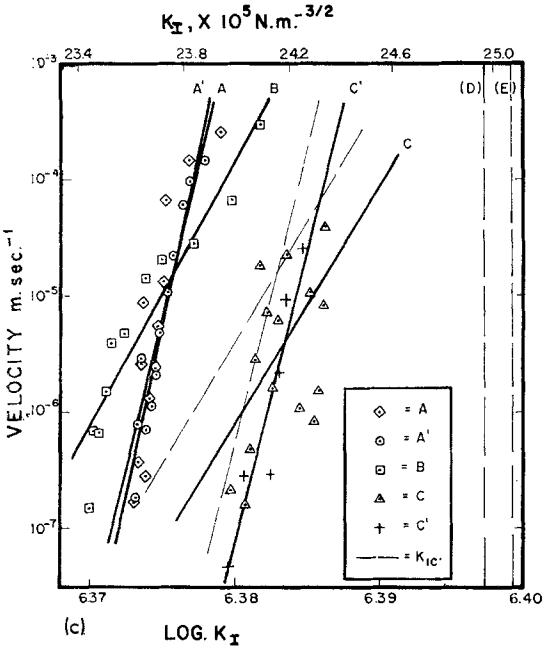

Figure 4 K_I-V diagrams at room temperature in air: (a) POCO AXZ, (b) POCO AXF-5Q, (c) Pyrolytic graphite.

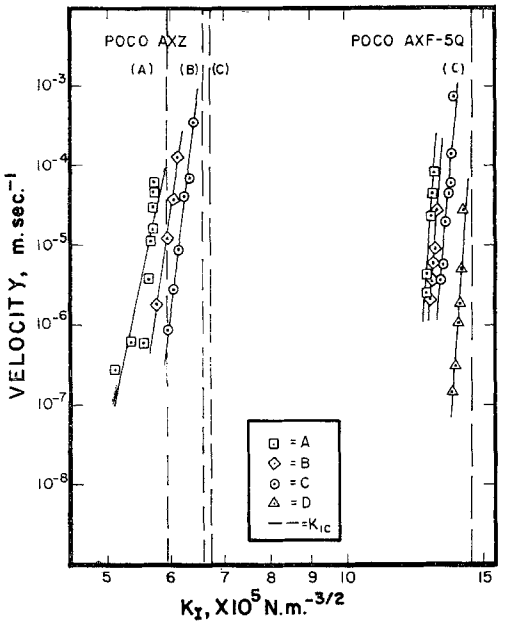

Figure 5 K_I-V diagrams for POCO AXZ and POCO AXF-5Q at 500°C in air.

3.3.3. Fractography

Examination of the fracture surface of isotropic graphite revealed slightly different fracture modes for each grade. Fig. 6a for POCO AXZ at room temperature shows that the fracture is partly intergranular and partly transgranular. In comparison, the fracture mode for POCO AXF-5Q was predominantly transgranular in nature (Fig. 6b); cleavage of filler particles has occurred exposing many spherically shaped closed pores and river patterns with rounded edges are abundant.

At 500°C the fracture surfaces of both isotropic graphites seemed less angular with a larger number of cleavage fractures of particles.

More cleavage fractures were also observed for both graphites in the rapid crack propagation region close to the end of the specimen.

Finally, the isotropic graphite samples tested at 500°C showed severe oxidation, many pits being formed on the surfaces.

In comparison to isotropic graphite, fracture in pyrolytic graphite progressed by the movement of the crack through basal plane layers in the "*a*" direction. River patterns, cleavage steps, and "tire tracks" were all observed. Fig. 6c shows the unevenness of the fracture surface, basal plane shearing is extensive and many fragments of material have peeled off the edges of the planes. In general, after moving approximately 1 cm from the notch tip, the crack front twisted into the material and delamination occurred.

4. Discussion

4.1. Fracture toughness, critical stress intensity factor

The room temperature value of K_{IC} for POCO AXF-5Q, 14.56 × 10^5 N $m^{-3/2}$, is in good agreement with Simpson's results of 14.9 × 10^5 N $m^{-3/2}$ (double torsion technique) and 15.4 × 10^5 N $m^{-3/2}$ (double cantilever beam) for the same material [3].

Table V indicates that the room temperature values of fracture toughness increase in the order POCO AXZ, AXF-5Q and pyrolytic graphite. The normalized parameter, K_{IC}, shows that this difference cannot be accounted for on the basis of the reduction in load-bearing area as a result of porosity. The pore size, shape and distribution are probably important as well.

Examination of fracture surfaces has shown that a greater proportion of transgranular fracture occurred in the case of POCO AXF-5Q than POCO AXZ and also when crack propagation was rapid compared with slow crack growth The spherical closed pores observed on the

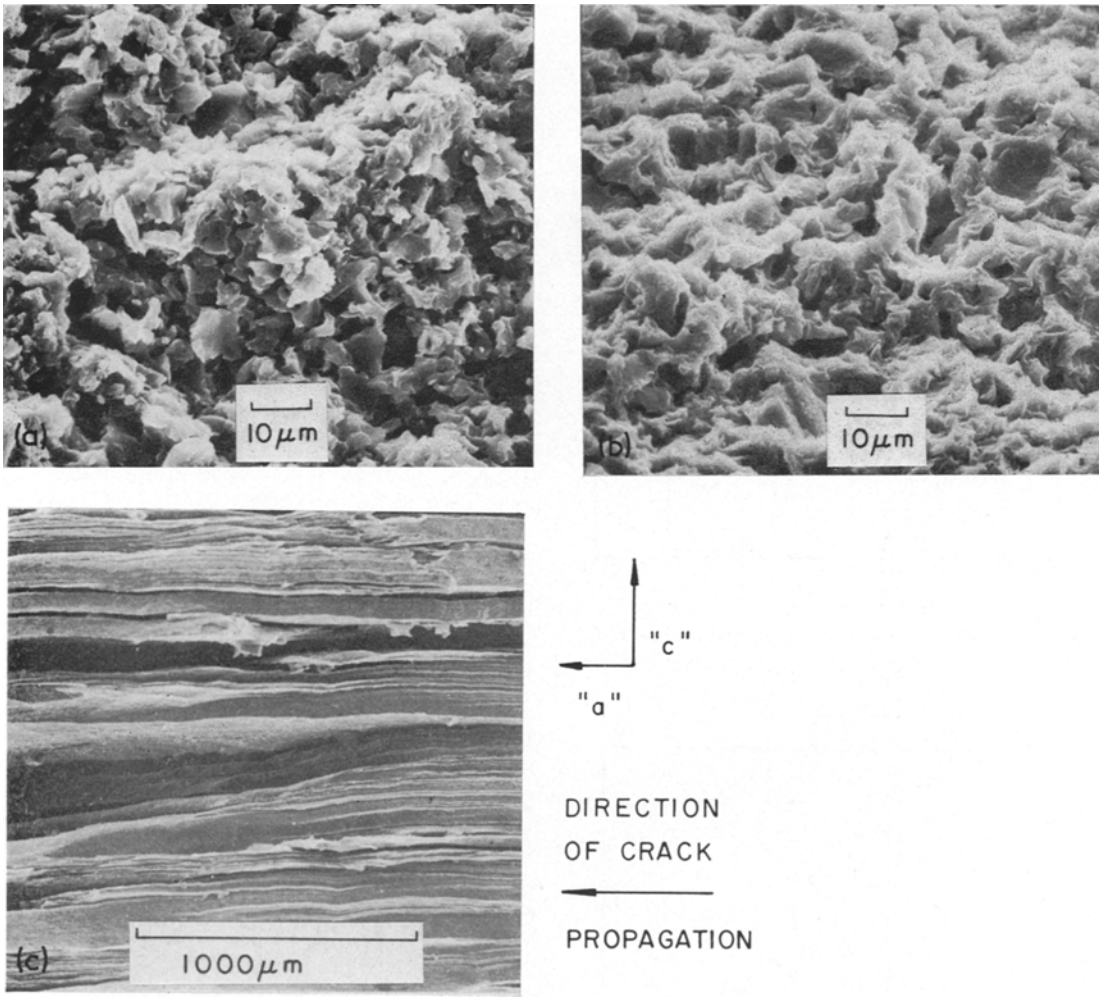

Figure 6 SEM photographs of room temperature fracture surfaces: (a) POCO AXZ; (b) POCO AXF-5Q; (c) Pyrolytic graphite.

fracture surfaces of POCO AXF-5Q would tend to blunt a propagating crack at various points along its length resulting in a reduction in the stress intensity. On the other hand, sharp angled interparticle pores at binder coke junctions may act as stress raisers, requiring a lower energy for crack propagation. An intergranular fracture mode may be expected to be easier to maintain in a material with a greater proportion of interconnected porosity such as POCO AXZ. The resultant lower fracture toughness would be countered in part, however, by the larger area of an intergranular rather than a transgranular fracture face.

The large value of fracture toughness for pyrolytic graphite can be explained by the very large amount of new surface area produced as a result of the complex fracture process.

4.2. Slow crack growth

The steep slopes of the K_I-V diagrams for all three graphites at room temperature resemble the third stage of crack growth in soda-lime glass [4], stage III being the region where crack growth is governed mostly by mechanical processes.

4.2.1. Isotropic graphites at room temperature

The results for POCO AXZ at room temperature indicate considerable variation in the stress

intensity required to propagate a crack in this material. This variability seems to occur not only from sample to sample but also in a particular specimen, as shown by the multiple load relaxation curves (Fig. 3b) and the discontinuous K_I-V curves (Fig. 4a).

In comparison to POCO AXZ, the load relaxation curves for POCO AXF-5Q usually consisted of a single continuous curve (Fig. 3a). The resultant K_I-V diagrams are very reproducible and there is a suggestion of a fatigue limit at K_I values of $\sim 13.8 \times 10^5$ N m$^{-3/2}$. The position and general shape of the diagrams are in good agreement with those of Simpson [3].

The reproducible K_I-V curves for POCO AXF-5Q are consistent with crack growth in a material having a uniform density and which does not tend to deflect the crack. In contrast, the variable K_I-V curves for POCO AXZ may reflect the more variable open pore volume and greater difficulty in preventing the growing crack from deviating from a straight path. The inhomogeneous nature of POCO AXZ indicates that the "microstructural obstacles" responsible for the discontinuous crack growth process may be nonuniform regions of intergranular porosity or possibly regions where the intergranular pores are less angular and so more likely to blunt the crack. Crack propagation would then occur in regions where the pores act as crack nuclei.

4.2.2. Isotropic graphites at 500° C

All the POCO AXZ specimens remained in the furnace for approximately the same time period, $3\frac{1}{2}$ h, so that the variation in the position of the K_I-V diagrams (Fig. 5) is again a reflection of the variability of the material. Although there was considerable background "noise" present at 500° C, the load relaxation curve appeared to consist of a single relaxation with no obvious discontinuities as at room temperature. Therefore, the K_I-V diagrams have a single continuous stage. The slope, $n = 63$ is considerably less than the room temperature value of 649. Also, fractographic evidence revealed a slight change in fracture mode at 500°C.

Specimens A, B, C, and D of POCO AFX-5Q were kept in the furnace at 500°C for $3\frac{1}{2}$, 3, $2\frac{1}{3}$ and $1\frac{1}{2}$ h, respectively. Therefore, the variable stress intensity observed for these samples may be due to either a reduction in the web thickness by surface oxidation or a general decrease in the stress that the material can support as a result of a reduction in load-bearing area through pore enlargement. Probably the same effect occurred with POCO AXZ, although more obscured by variability of the material. This is shown to a certain extent by the general shift of the K_I-V diagrams to lower stress intensities at 500°C compared to room temperature.

The slope, $n = 128$ for POCO AXF-5Q is significantly less than the room temperature value of 218, again indicating thermal and/or environmental assistance of crack growth at high temperatures.

4.2.3. Pyrolytic graphite at room temperature

The position of the K_I-V curves (Fig. 4c) is fairly reproducible and seems consistent with a relatively homogeneous microstructure; the initial straightness of the crack path supports this. However, the structure appears to be "semihomogeneous" in that "microstructural obstacles" are encountered by a moving crack. The effectiveness of these obstacles varies as the crack may be brought to a complete halt ($n \sim 500$) or merely slowed down ($n \sim 200$). The latter is well shown in Fig. 3c for the final acceleration in curve C. The microstructural obstacles are probably cone interfaces where basal plane edges overlap, the degree of mismatch or overlap controlling their effectiveness.

The apparent change in fracture mode on catastrophic crack propagation is believed to be due also to the wavy nature of the basal planes. Any stress applied to a stack of wavy planes has resolved components parallel and perpendicular to the planes. Thus, crack growth in the double torsion specimen of pyrolytic graphite probably occurred by a combination of mode I opening and mode III shearing. The mode III failure would be more apparent at longer distances from the notch tip where the crack front is no longer constrained to propagate through the basal planes.

5. Conclusions

Slow crack growth studies have shown that little slow crack growth occurs in graphite at room temperature except at very high fractions of the critical stress intensity. The stress intensity-crack velocity diagrams resemble the third stage of crack growth in soda-lime glass, so that slow crack growth in graphite at room temperature is determined mostly by mechanical failure. The form of these diagrams reflect microstructural

features in the material controlling mechanical failure.

Thermal and/or environmental assistance of slow crack growth in graphite occurs at 500°C. However, the steep nature of the K_I-V curves indicate that delayed failure is still determined mainly by mechanical processes.

Acknowledgements

The writers thank Dr O. J. Whittemore, Jun, and Kunio Aihara of the University of Washington, Seattle for the mercury porosimetry results. Acknowledgement is made of financial assistance from the Atomic Energy of Canada Ltd.

References

1. R. J. DIEFENDORF, in "Proceedings of the 4th Conference on Carbon, Buffalo, 1959", (Pergamon Press, New York, 1960) p. 489.
2. B. J. S. WILKINS, *J. Amer. Ceram. Soc.* **54** (1971) 593.
3. L. A. SIMPSON, Atomic Energy of Canada, Whiteshell, Manitoba, unpublished data.
4. S. M. WIEDERHORN, in "Mechanical and Thermal Properties of Ceramics", edited by J. B. Wachtman Jun, N.B.S. Special Publication No. 303, Washington (1969) p. 217.
5. P. WAGNER, J. A. O'ROURKE and P. E. ARMSTRONG, *J. Amer. Ceram. Soc.* **55** (1972) 214.
6. H. M. BLAES, J. D. MCCLELLAND and J. H. RICHARDSON, in "10th Biannual Conference on Carbon, Bethlehem, Pa., 1971", American Carbon Committee, Pennsylvania State University, p. 225.
7. S. SPINNER and W. E. TEFFT, *ASTM Proc.* **61** (1961) 1221.
8. G. PICKETT, *ibid* **45** (1945) 846.
9. A. G. EVANS, *J. Mater. Sci.* 7 (1972) 1137.
10. D. P. WILLIAMS and A. G. EVANS, *J. Testing and Evaluation* **1** (1973) 264.
11. P. H. HODKINSON, M.Sc. Thesis, University of British Columbia, Vancouver (November 1973).
12. B. W. GONSER, Ed., "Modern Materials", Vol. 7 (Academic Press, London, 1970).

Received 1 August and accepted 15 October 1974.